catalysts

MDPI

Article

Undoped and Fe-Doped Anatase/Brookite TiO_2 Mixed Phases, Obtained by a Simple Template-Free Synthesis Method: Physico-Chemical Characterization and Photocatalytic Activity towards Simazine Degradation

Stefano Gervasi [1,†], Nicola Blangetti [1,†], Francesca S. Freyria [1,*], Salvatore Guastella [1] and Barbara Bonelli [1,2,*]

[1] Department of Applied Science and Technology and INSTM Unit of Torino-Politecnico, Corso Duca degli Abruzzi 24, I-10129 Torino, Italy
[2] Interdepartmental Centre Polito^{BIO}Med Lab, Corso Duca degli Abruzzi 24, I-10129 Torino, Italy
* Correspondence: francesca.freyria@polito.it (F.S.F.); barbara.bonelli@polito.it (B.B.); Tel.: +39-011-0904719 (B.B.)
† These authors contributed equally to this work.

Abstract: For the first time, Fe-doping (0.05, 1.0, and 2.5 wt.% Fe) was performed on a high-surface-area anatase/brookite TiO_2 by adopting a simple template-free sol-gel synthesis followed by calcination at a mild temperature. The powders' textural and surface properties were characterized by following a multi-technique approach. XRD analysis showed that the anatase/brookite ratio slightly varied in the Fe-doped TiO_2 (from 76.9/23.1 to 79.3/22.7); Fe doping noticeably affected the cell volume of the brookite phase, which decreased, likely due to Fe^{3+} ions occupying interstitial positions, and retarded the crystallite growth. N_2 sorption at −196 °C showed the occurrence of samples with disordered interparticle mesopores, with an increase in the specific surface area from 236 $m^2\ g^{-1}$ (undoped TiO_2) to 263 $m^2\ g^{-1}$ (2.5 wt.% Fe). Diffuse Reflectance UV-Vis spectroscopy showed a progressive decrease in the bandgap energy from 3.10 eV (undoped TiO_2) to 2.85 eV (2.5 wt.% Fe). XPS analysis showed the presence of some surface Fe species only at 2.5 wt.% Fe, and accordingly, the ζ-potential measurements showed small changes in the pH at the isoelectric point. The photocatalytic degradation of simazine (a persistent water contaminant) both under UV and simulated solar light was performed as a probe reaction. Under UV light, Fe-doping improved simazine degradation in the sample at 0.05 wt.% Fe, capable of degrading ca. 77% simazine. Interestingly, the undoped TiO_2 was also active both under UV and 1 SUN. This is likely due to the occurrence of anatase/brookite heterojunctions, which help stabilize the photogenerated electrons/holes.

Keywords: TiO_2 polymorphs; anatase/brookite heterojunctions; Fe-doped TiO_2; simazine degradation; detoxification

Citation: Gervasi, S.; Blangetti, N.; Freyria, F.S.; Guastella, S.; Bonelli, B. Undoped and Fe-Doped Anatase/Brookite TiO_2 Mixed Phases, Obtained by a Simple Template-Free Synthesis Method: Physico-Chemical Characterization and Photocatalytic Activity towards Simazine Degradation. *Catalysts* **2023**, *13*, 667. https://doi.org/10.3390/catal13040667

Academic Editor: Nina Kaneva

Received: 28 February 2023
Revised: 17 March 2023
Accepted: 27 March 2023
Published: 29 March 2023

1. Introduction

Along with ZnO, TiO_2 is one of the most studied semiconductors, with actual and potential applications in various fields. These applications include photocatalytic processes, during which the following events take place upon TiO_2 interaction with the light of proper energy [1,2]:

$$TiO_2 + h\nu \rightarrow e^-_{CB} + h^+_{VB} \quad (1)$$

$$e^-_{CB} + O_2 + H^+ \rightarrow HO_2\bullet \quad (2)$$

$$e^-_{CB} + HO_2\bullet + H^+ \rightarrow H_2O_2 \quad (3)$$

$$2e^-_{CB} + O_2 + 2H^+ \rightarrow H_2O_2 \quad (4)$$

$$h^+_{VB} + H_2O \rightarrow HO\bullet + H^+ \quad (5)$$

$$2HO\bullet \rightarrow H_2O_2 \quad (6)$$

$$H_2O_2 + h\nu \rightarrow 2HO\bullet \quad (7)$$

$$H_2O_2 + e^-_{CB} + H^+ \rightarrow HO\bullet + H_2O \quad (8)$$

According to Reactions (1)–(8), valence band (VB) electrons are promoted to the conduction band (CB, e^-_{CB}), and simultaneously holes are produced in the VB (h^+_{VB}): the so photogenerated charge carriers (e^-_{CB} and h^+_{VB}) undergo several reactions producing (highly oxidizing) radical species (e.g., HO•).

From a practical point of view, photocatalytic applications of TiO_2 are usually hampered by two major drawbacks: (i) the fast recombination of photogenerated charge carriers [3], which decreases the overall yield [4,5] and (ii) the poor absorption of the solar spectrum, which contains only a minor fraction of UV light (ca. 4%), whereas the three most common polymorphs of TiO_2, namely anatase, brookite, and rutile, have average bandgap energies (E_g) in the UV range (of ca. 3.2, 3.4 and 3.0 eV, respectively [6,7]). By tailoring the semiconductor properties, different strategies can be adopted to cope with such issues: for instance, (i) the production of composites containing heterojunctions between TiO_2 and other substances [8,9] or between TiO_2 polymorphs [10,11] can improve the lifetime of photogenerated charge carriers, and (ii) the doping with heteroatoms can red shift the TiO_2 absorption edge and improve its absorption of solar light [12,13].

Concerning the presence of inter-polymorph heterojunctions to stabilize the charge carriers in undoped TiO_2, anatase/rutile heterojunctions are generally considered responsible for the superior photocatalytic activity of Degussa P25, the commercial product used as a benchmark in most studies [14,15]. Currently, there is a growing interest in anatase/brookite heterojunctions [16–18]. Indeed, we have observed that such heterojunctions can be responsible for the fair photocatalytic activity of an anatase/brookite TiO_2 mixed phase towards the degradation of the herbicide N-phenylurea, both under UV and simulated solar light [11].

Concerning doping with heteroatoms, Fe is an earth-abundant, non-toxic element, and can be successfully introduced to different types of materials, such as alumino-silicates, due to the similar charge to radius ratio of Fe^{3+} and Al^{3+} [19–21]. Concerning semiconductors, the effects of Fe doping are exploited, for instance, in ZnO and TiO_2. With ZnO, several effects are observed, such as the formation of Fe^{2+} species, the segregation of Zn/Fe mixed spinels, and the occurrence of interesting optical and magnetic properties [22–24]. Concerning the effect of Fe doping in TiO_2, which is the subject of this study, it is known to shift the absorption edge towards the visible range [25–28] by forming new levels within the TiO_2 bandgap (Scheme 1).

In the bulk, the Fe species may also act as traps for the photogenerated e^-_{CB} and h^+_{VB} (Scheme 1), avoiding their recombination and giving rise to the following reactions [29]:

$$Fe^{3+} + e^-_{CB} \rightarrow Fe^{2+} \quad (9)$$

$$Fe^{2+} + Ti^{4+} \rightarrow Fe^{3+} + Ti^{3+} \quad (10)$$

$$Fe^{3+} + h^+_{VB} \rightarrow Fe^{4+} \quad (11)$$

$$Fe^{4+} + OH^- \rightarrow Fe^{3+} + HO\bullet \quad (12)$$

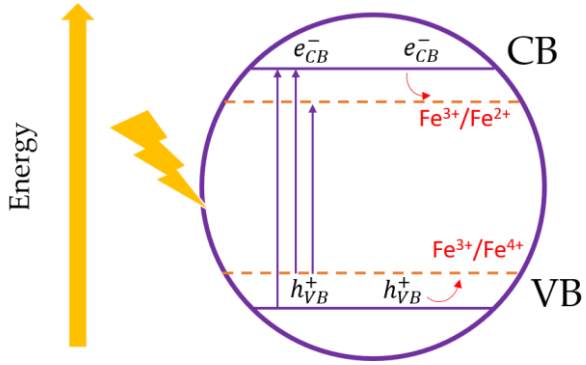

Scheme 1. Processes occurring in Fe-doped TiO_2 upon interaction with light (adapted from Ref. [29]).

In the presence of TiO_2, the photogenerated h^+_{VB} can react with Fe^{3+} species to produce (unstable) Fe^{4+} species, which can provide additional HO• species, according to Equations (11) and (12).

Moreover, Fe-species on the TiO_2 surface in the presence of H_2O_2 can undergo Fenton- and Fenton-like processes, well known in the homogeneous phase but possible in the heterogeneous phase as well. In such processes, both Fe^{3+} (Equation (13)) and Fe^{2+} (Equation (14)) ions may react with H_2O_2 to form radicals [30,31], which further react with H_2O_2 according to the following reactions that can be exploited to degrade, for instance, water pollutants:

$$Fe^{3+} + H_2O_2 \rightarrow Fe^{2+} + H^+ + HO_2\bullet \quad (13)$$

$$Fe^{2+} + H_2O_2 \rightarrow Fe^{3+} + OH^- + HO\bullet \quad (14)$$

$$HO\bullet + H_2O_2 \rightarrow H_2O + HO_2\bullet \quad (15)$$

$$HO_2\bullet + H_2O_2 \rightarrow HO\bullet + H_2O + O_2 \quad (16)$$

$$\text{Pollutant} + HO\bullet \rightarrow \text{degradationproducts} \quad (17)$$

Typically, Fe^{3+} species reacts more slowly (Equation (13)) than Fe^{2+} species (Equation (14)) [32], but in the presence of light with $\lambda < 600$ nm, the photo-Fenton process takes place, during which Fe^{3+} species is reduced to (more active) Fe^{2+} species, yielding HO• radicals [20,33]:

$$Fe(OH)^{2+} + h\nu \rightarrow Fe^{2+} + HO\bullet \quad (18)$$

$$Fe^{3+} + H_2O + h\nu \rightarrow Fe^{2+} + HO\bullet + H^+ \quad (19)$$

$$H_2O_2 + h\nu \rightarrow 2HO\bullet \quad (20)$$

Photocatalysis and Fenton-like reactions belong to the class of the so-called Advanced Oxidations Processes (AOPs), i.e., those methods that, through the production of very oxidizing species, allow degradation of several organic (and inorganic) substances, yielding by-products or mineralization [1,2]. By these methods, it would be possible to also treat persistent pollutants and/or micropollutants (present at very low concentrations), which can escape traditional water treatment plants [31,34–36], such as simazine (Scheme 2). Simazine is a herbicide of the triazine family. Although it has been banned since 1991 in Italy and Germany [37] and since 2004 in most of the other European countries [38], Simazine is still detected in some surface and ground waters, as traditional water treatment plants are unable to remove it. Recently, along with atrazine, a pesticide of the same family (Scheme 2), simazine has been banned in Hawaii and other U.S. territories [39], as several reports pointed out that it is a potential endocrine disruptor, which can lead to reproductive disorders and be toxic to humans and wildlife [38].

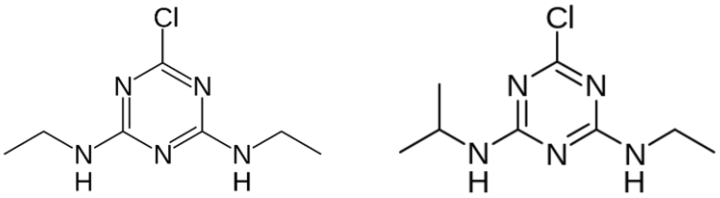

Simazine Atrazine

Scheme 2. The chemical structures of simazine (IUPAC name: 6-chloro-N2,N4-diethyl-1,3,5-triazine-2,4-diamine) and atrazine (IUPAC name: 6-Chloro-N2-ethyl-N4-(propan-2-yl)-1,3,5-triazine-2,4-diamine).

Due to its chemical stability and persistence [40], simazine is the second most detected herbicide/pesticide in waters of the Western world. Concerning the distribution of the pollutant in Europe, in 2017, the analysis of over 7000 sites including both surface and groundwater all over Europe showed that simazine was the third among herbicides/pesticides detected in surface waters and the second among those detected in groundwater [41]. The persistence of simazine in soils or a natural habit can make it a dangerous pollutant. Indeed, it is considered a pollutant of environmental concern [42], due to its persistence, stability, environmental distribution, very high toxicity for aquatic life and suspected carcinogenicity.

Concerning non-reactive methods for simazine removal, adsorption on widely available, low-cost adsorbents [43,44] suffers from the drawback of their regeneration. Concerning reactive methods, different solutions have been exploited. For instance, Sun et al. [45] studied the chemical degradation of simazine by diatomite-supported NZVI (Nanoscale Zero Valent Iron). For the photocatalytic removal of simazine through AOPs, only a few studies imply the use of visible or solar light and engineered composites of graphene-like materials [46,47], whereas most studies implying the use of TiO_2 are carried out under UV light [48–50].

In this work, for the first time, we synthesized and characterized samples of Fe-doped anatase/brookite high-surface-area mesoporous TiO_2 through a simple procedure based on pH control followed by calcination at a mild temperature (namely 200 °C); an undoped anatase/brookite (AB sample) TiO_2 was also obtained for comparison by slightly modifying a literature procedure [51]. On the one side, the adopted synthesis is more sustainable than other methods, implying the use of organic templates and the need for high calcination temperature to obtain high-surface-area mesoporous TiO_2 [10,52–55]; on the other side, it allows obtaining an anatase/brookite mixed phase that we already proved active under both UV and solar illumination [11]. To the best of our knowledge, it is the first time such a method [11,51] has been applied to obtain Fe-doped TiO_2: by adding proper amounts of $FeCl_3 \times 6H_2O$, three nominal Fe-contents have been studied, corresponding to 0.05, 1.0, and 2.5 wt.% Fe in the AB_0.05_Fe, AB_1.0_Fe, and AB_2.5_Fe samples, respectively. After the physico-chemical characterization of their textural and surface properties, the photocatalytic degradation of simazine under UV and solar light was used as a probe reaction in different conditions, namely the absence/presence of H_2O_2 in stoichiometric amount, as too high H_2O_2 concentration may lead to adverse effects, by consuming HO• radicals and producing less reactive HO_2• radicals (Equation (15)) [55].

2. Results and Discussion

2.1. Physico-Chemical Characterization

Figure 1a reports the X-ray Diffraction (XRD) patterns of the studied samples, and the corresponding results of the Quantitative Phase Analysis (QPA) is reported in Table 1. The undoped AB sample shows the peaks of both anatase (A, main peaks at ca. 25.2 and ca. 48.1 2θ values, ICDD card no. 01-073-1764) and brookite (B, main peaks at ca. 25.2, 25.5 and 30.6 2θ values, COD card No 96-900-4141), with a relative abundance of 77.7 wt.% and 22.3 wt.%, respectively. Doping with Fe does not lead to the appearance of other phases

besides anatase and brookite nor to a consistent change in their abundance (Table 1), likely due to the low Fe content [52–55].

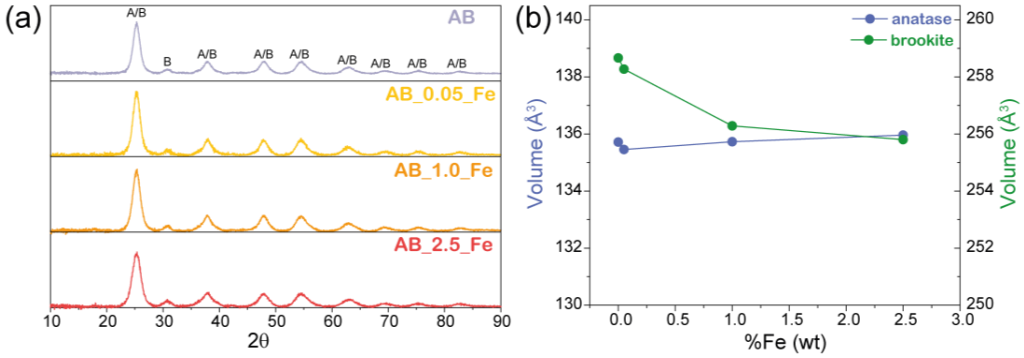

Figure 1. XRD patterns of the studied powder samples. The main peaks of anatase and brookite are labelled as A and B, respectively (**a**); values of the cell volumes of anatase and brookite versus the nominal Fe content (wt.%) (**b**).

Table 1. Some relevant physico-chemical properties of the studied samples, as obtained using XRD followed by Rietveld refinement [a] and Williamson-Hall method, [b] N_2 isotherms at −196 °C, [c] and DR UV-Vis spectroscopy. [d] A = anatase; B = brookite.

Sample	QPA Results: (Phase wt.%) [a]	Crystallite Size (±nm) [b]	BET SSA ($m^2\ g^{-1}$) [c]	V_{tot} ($cm^3\ g^{-1}$) [c]	Extrapolated/ Tauc's Plot Determined E_g Values (eV) [d]
AB	77.7 A 22.3 B	5.2 (0.2) A 7.1(0.1) B	236	0.293	3.30/ 3.10
AB_0.05_Fe	76.9 A 23.1 B	5.0 (0.1) A 5.6 (0.2) B	233	0.286	3.22/ 3.07
AB_1.0_Fe	79.3 A 20.7 B	4.7 (0.1) A 6.0 (0.2) B	243	0.253	3.10/ 2.92
AB_2.5_Fe	78.4 A 21.6 B	4.4 (0.1) A 5.7 (0.2) B	263	0.245	3.01/ 2.85

The broad peaks show that the AB powder has a low crystallinity degree, likely due to the low calcination temperature (namely 200 °C), and accordingly, the crystallite sizes are small (ca. 5.2 and 7.1 nm for anatase and brookite, respectively). As shown in Table 1, the crystallite size of both phases slightly decreases in the Fe-doped samples, in agreement with previous work on Fe-doped anatase/brookite TiO_2, where the presence of Fe^{3+} ions was found to retard the crystallite growth [56].

Figure 1b, instead, shows that the cell volume of brookite decreases with the Fe content, whereas the anatase cell volume is less affected by doping (Figure 1b) indicating that the effects of Fe-doping are more noticeable on the brookite phase. The crystallite size of both phases slightly decreases (Table 1), especially at the minimum amount of doping. Concerning the type of process when Fe^{3+} ions are inserted into the TiO_2 lattice, in a previous work on Fe-doped anatase/brookite/rutile TiO_2, using a reverse-micelle sol-gel method to incorporate Fe in both anatase and brookite [53], an initial expansion of both the anatase and brookite cell volumes occurred at 1.0 wt.% Fe, and then the cell volumes decreased at a Fe content above 1.0 wt.%. The former phenomenon was ascribed to the isomorphic substitution of Ti^{4+} by Fe^{3+} ions, while the latter was caused by the occupation of interstitial sites by (extra) Fe^{3+} ions. In this case, the peculiar synthesis procedure seems to help the latter process, which, in turn, mainly affects the brookite phase, characterized by a more disordered and open structure than anatase [7].

Figure 2 reports some selected FESEM micrographs of the studied powders: small nanoparticles are observed with four samples, which are all characterized by a high aggregation/agglomeration degree. The nanoparticles size and shape are mostly unaffected by the presence of Fe, and their size agrees with a previous microscopic characterization of an undoped anatase/brookite TiO_2, obtained by the same synthesis method of the AB sample, showing that the nanoparticles size is of the order of the crystallite size [11]. The corresponding EDX-determined elemental maps are reported in Figure S1 for the Fe-doped samples, showing a homogeneous distribution of Fe in the synthesized powders.

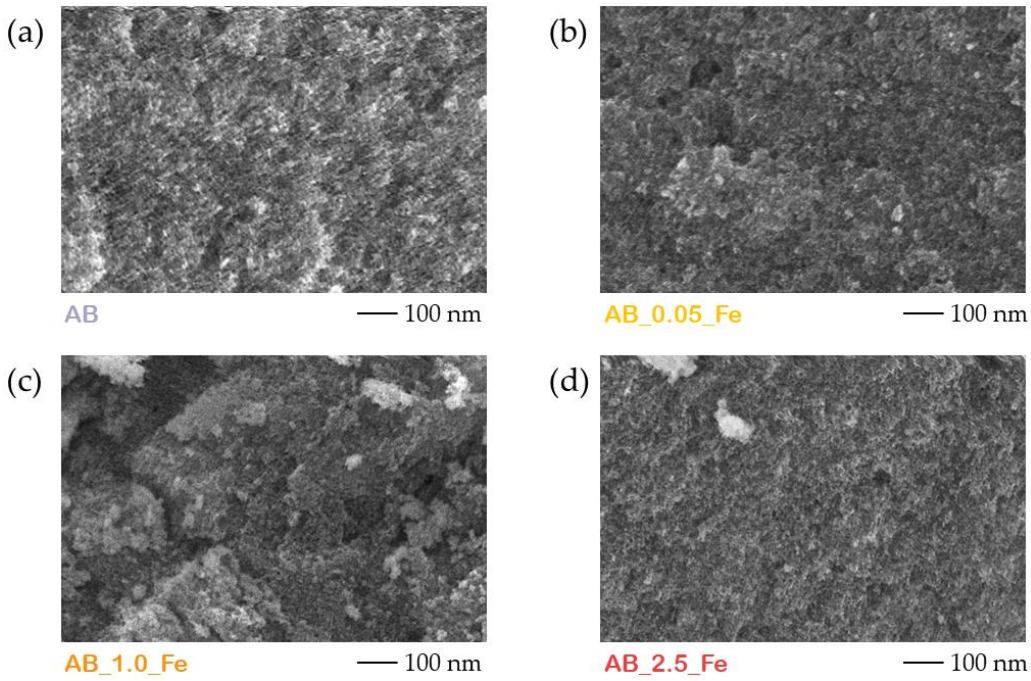

Figure 2. Selected FESEM micrographs of the AB (**a**), AB_0.05_Fe (**b**), AB_1.0_Fe (**c**) and AB_2.5_Fe (**d**) powder samples, showing nanoparticles with similar size and morphology, as well as a high degree of agglomeration/aggregation.

Figure 3 reports the N_2 adsorption/desorption isotherms measured at −196 °C on the studied samples: all the studied powders showed type IV isotherms with H2 hysteresis loops, indicating the occurrence of interconnected mesopores of different shapes and sizes. The adopted synthesis procedure likely leads to disordered inter-particle mesopores, as also shown by the Pore Size Distribution (PSD) curves reported in the insets. The AB, AB_1.0_Fe, and AB_2.5_Fe samples have a sharp PSD with a maximum at ca. 4.0 nm, whereas the AB_0.05_Fe sample has a broader PSD, likely due to some aggregation/agglomeration phenomena (Figure 2). The PSD curves show that the samples' pore diameters largely exceed simazine's molecular dimensions (ca. 1.1 × 0.75 nm [57]), thus diffusion problems during the photocatalytic tests should be avoided. Interestingly, the four powders are characterized by high specific surface area (SSA) values (Table 1). Except sample AB_0.05_Fe, which has an SSA very close to that of the (undoped) AB sample likely due to the low Fe content, the SSA is seen to increase with Fe doping.

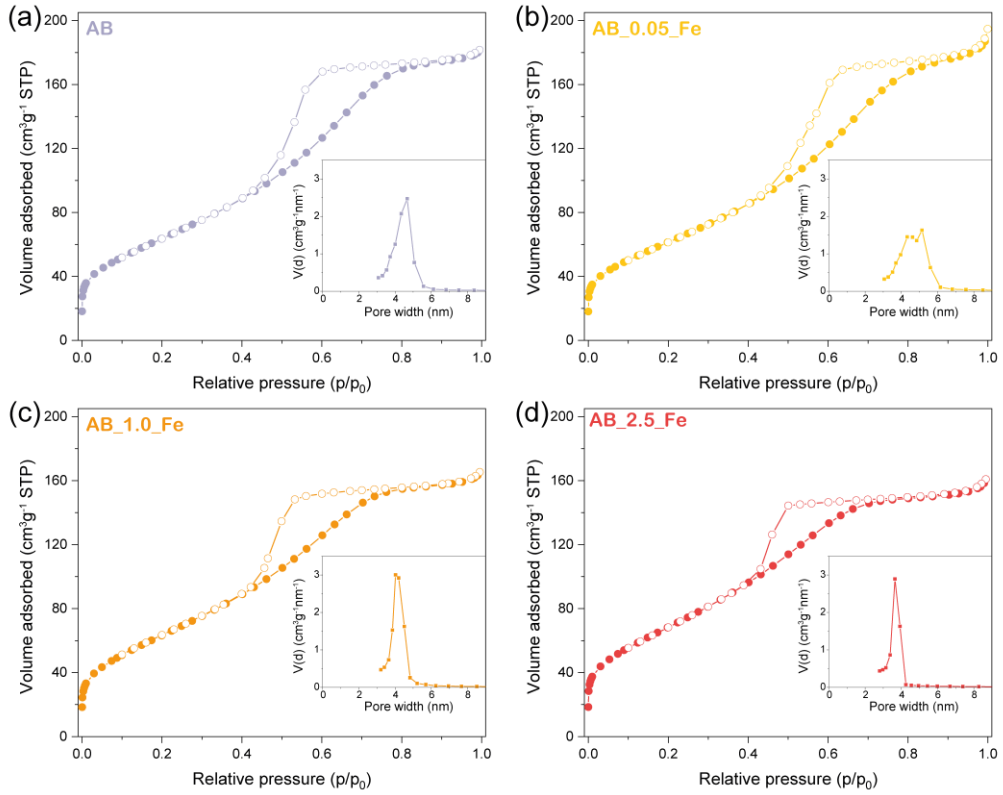

Figure 3. N_2 adsorption/desorption isotherms at − 196 °C on the AB (**a**), AB_0.05_Fe (**b**), AB_1.0_Fe (**c**) and AB_2.5_Fe (**d**) samples; full and empty symbols refer to adsorption and desorption run, respectively. Insets: PSD curves, as obtained by applying the BJH method to the isotherm's desorption branch.

Figure 4a reports the DR UV-Vis spectra of the studied samples: with the AB sample, the typical electronic transitions due to the charge transfer (CT) from O^{2-} to Ti^{4+} in undoped TiO_2 are observed, along with an Urbach tail (inset), which will be discussed later. With the AB_0.05_Fe sample, a band at ca. 235 nm can be assigned to CT from O^{2-} to Ti^4 ions in an environment perturbed by the presence of Fe^{3+} ions [58]. Such an effect is not so noticeable with the other two powders and could be due to a stronger effect of Fe substitution on the TiO_2 matrix at low Fe content. Doping with Fe brings a red shift of the absorption onset, surely related to bulk Fe doping, in agreement with the reported XRD patterns, which also brings about a decrease of the energy gap, vide infra. The formation of interband states due to Fe doping can be appreciated in the UV-Vis spectra of the doped samples (inset to Figure 4a).

With Fe-doped TiO_2 obtained by different (template-assisted) sol-gel techniques, the formation of surface Fe-oxohydroxo cluster was observed, especially at 2.5 wt.% Fe. Correspondingly, XPS was able to detect the presence of some surface Fe species [53]. With the present samples, instead, XPS analysis detected the presence of surface Fe species only with the AB_2.5_Fe sample (Figure S2). As an Fe/Ti atomic ratio equal to 0.071 was measured by XPS, higher than the nominal value of 0.037, this indicates that at higher Fe content, some Fe oxyhydroxide species may occur; indeed, a signal was observed at ca. 480 nm (asterisk, Figure 4a), corresponding to a signal at 2.55 eV in the related Tauc's plot (asterisk, Figure 4b). XPS also detected some Cl traces (0.6 at.%; Cl/Fe atomic ratio of 0.46).

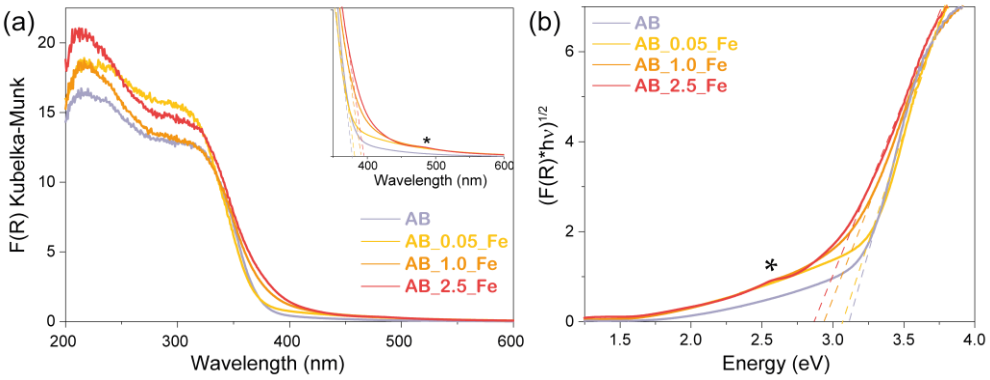

Figure 4. DR UV-Vis spectra of the studied powders (**a**) and corresponding Tauc's plot, as obtained by assuming a behaviour of indirect semiconductors (**b**). Asterisks at 480 nm (inset to Figure 4a) and at 2.55 eV (Figure 4b) refer to evidence of the formation of Fe oxyhydroxide species.

Concerning the bandgap energy, since the samples contain not only anatase (an indirect semiconductor) but also brookite (a direct semiconductor), the bandgap values (E_g) of the powders have been calculated both by applying the Tauc's plot method (Figure 4b) for an indirect semiconductor $((F(R) \times h\nu)^{1/2}$ and by extrapolation of the spectra absorption onset (dashed lines in Figure 4a). The obtained E_g values are reported in Table 1: slightly smaller values are obtained by Tauc's plot method, likely due to the indirect semiconductor assumption, but generally Fe brings about a decrease in the E_g values. Analysis of the Tauc's plot curves shows that the AB (undoped) sample is characterized by an Urbach tail, namely an exponential part in the energy spectrum of the absorption coefficient that may appear near the optical band edge in amorphous, disordered, and crystalline materials, including undoped TiO_2 mixed phases [59]. Figure S3 reports a comparison of the AB spectrum with a spectrum of Degussa P25, showing that the former sample extends its absorption towards longer wavelengths. Such phenomenon allows absorption of a broader range of light energy; therefore, it is useful in photocatalytic applications, especially under solar illumination (vide infra).

Figure 5 reports the ζ-potential curves of the studied powders in water: they are positively and negatively charged, respectively, above and below a pH of ca. 5.00–6.00. According to the literature, the pH at the isoelectric point (pH_{IEP}) of brookite and anatase is around 5.10 and 6.00, respectively [60], and Fe_2O_3 has pH_{IEP} values in the 5.80–6.20 range [61]. The pH_{IEP} of the undoped AB sample is very close to that of brookite, and the pH_{IEP} of the AB_1.0_Fe and AB_2.5_Fe samples is not much affected by Fe-doping, in agreement with the low Fe content. Concerning the AB_0.05_Fe sample, the slightly higher pH_{IEP} value may be due to the presence of a higher abundance of exposed anatase nanoparticles, due to a kind of heterogeneity induced by the agglomeration/aggregation phenomena, already evidenced by FESEM (Figure 2). Such agglomeration/aggregation phenomena may also occur in aqueous phase: indeed, according to the literature, stable nanoparticles suspension are characterized by values of surface charges above +30 mV and below −30 mV (dotted lines) [62,63], whereas the studied powders have lower (in absolute value) surface charges in a broad pH range.

The physico-chemical characterization reported so far showed that the adopted synthesis procedure led to the production of mesoporous anatase/brookite TiO_2 samples, occurring as highly agglomerated/aggregated nanoparticles and that the Fe-doping mainly occurred in the TiO_2 bulk, especially at low Fe content, with a more noticeable effect on the crystallographic parameters of the brookite phase.

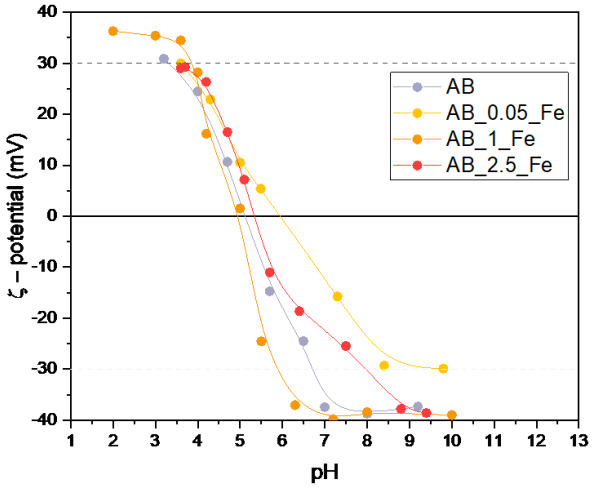

Figure 5. ζ-potential curves of the studied powders. The dashed lines at ζ = + 30 mV and −30 mV indicate the upper and lower values of surface charge above and below which stable suspensions of nanoparticles occur according to the literature [55,56].

2.2. Simazine Degradation under UV Light

Figure 6 reports the results of the photocatalytic tests obtained after 3 h illumination under UV light. The parent simazine solution (spectra taken at t = 0 min) has two bands at 222 and 265 nm, assigned to $\pi \rightarrow \pi^*$ and $n \rightarrow \pi^*$ electronic transitions, respectively [64]; under UV illumination, several new bands also form in the presence of the (undoped) AB sample, showing that the studied samples are photocatalytically active towards simazine degradation. Here, it is considered as a probe reaction, and the mechanisms of simazine degradation have already been addressed in the literature and will be used as a reference in this paper.

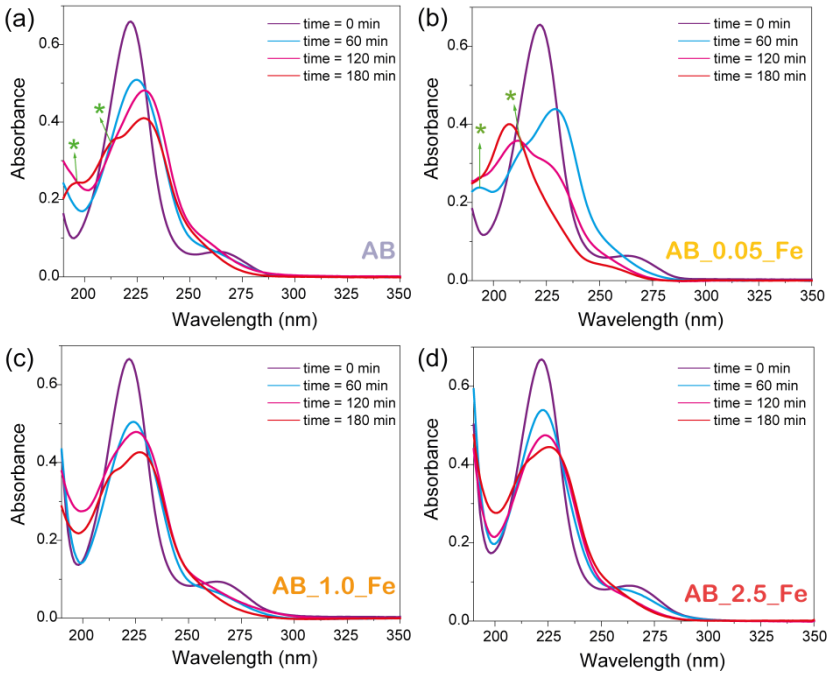

Figure 6. UV-Vis spectra of the supernatant solutions obtained after 60, 120 and 180 min under UV illumination in the presence of 1 g L^{-1} AB (**a**), AB_0.05_Fe (**b**), AB_1.0_Fe (**c**) and AB_2.5_Fe (**d**) photocatalyst (t = 0 min refers to the spectrum of the fresh 1.73 10^{-5} M simazine solution). Green asterisks indicate possible bands of cyanuric acid.

It has to be remarked that simazine is an extremely stable molecule, due to the energy gap between its frontiers orbitals [65] and, thus, its mineralization:

$$C_7H_{12}ClN_5 + 16O_2 \rightarrow 5HNO_3 + HCl + 7CO_2 + 3H_2O \quad (21)$$

is hardly achieved. Indeed, AOPs mostly lead to the formation of cyanuric acid (Scheme 3), which is not as toxic as the parent molecule [66] and has a characteristic UV spectrum in water, with a more intense band at 213 nm and a shoulder at 193 nm [67] (green asterisks in Figure 6). Typically, before the formation of cyanuric acid, simazine molecules (and triazines, in general) undergo dealkylation (i.e., loss of the lateral chains) and dechlorination (i.e., substitution of the Cl atom by an OH group) [50]. In the aqueous phase, dealkylation brings about a blue shift of the simazine 222 nm band (and the disappearance of the 265 nm band), whereas dechlorination brings about a red shift of the 222 nm band. The substitution of Cl, although without leading to mineralization, is considered a strategy of detoxification, i.e., the production of less toxic products [68,69], which can be a potential solution when mineralization is hard to achieve.

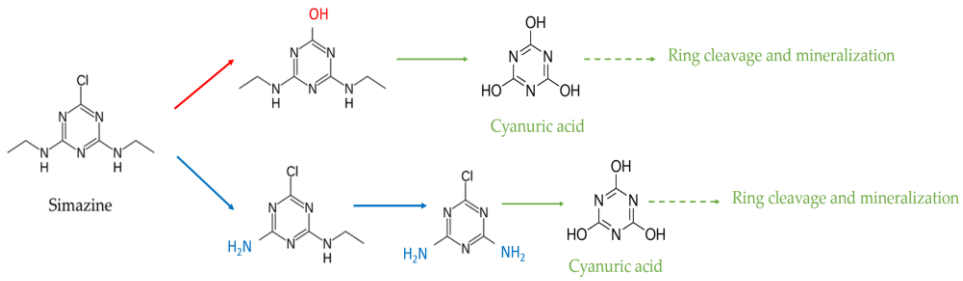

Scheme 3. Oxidative degradation pathways of simazine adapted from refs. [59,61].

In the following discussion, due to the complicated interpretation of UV-Vis spectra and since we are considering simazine degradation simply as a probe reaction to further characterize the studied samples, we will consider the intensity of the spectra at 222 nm: obviously, simazine by-products could absorb in that spectral range and, thus, the overall percentage of degraded simazine could be underestimated. It has to be remarked that if the intensity of the (broad) 266 nm band was considered, higher simazine degradation percentages were calculated, and we will consider an error of ±10% on the percentage of simazine degradation.

Figure S4a reports the results of the tests of UV photolysis, showing that in the adopted experimental conditions ca. 41% simazine was degraded, but the bands of cyanuric acid were not observed. Figure S4b reports the photocatalytic results in the presence of 1 g/L mesoporous anatase with a SSA of 150 $m^2\ g^{-1}$ and a bandgap of 3.20 eV [11,60], which was taken as a benchmark as our samples had anatase contents in the 77.7–79.3% range (Table 1). With the mesoporous anatase, dechlorination took place, likely due to the formation of 4,6-diamino-2-hydroxy-1,3,5-triazine (band at 229 nm [70]), which then transforms into a more hydroxylated product (isosbestic point), but the bands of cyanuric acid are not clearly distinguishable. With the AB powder (Figure 6a), firstly a red shift of the 222 nm band is observed, indicating the occurrence of a dechlorination process. Then, the bands of cyanuric acid (green asterisks) appear after 180 min illumination, indicating that with the undoped sample, the formation of cyanuric acid is accelerated, as compared to mere photolysis. With the AB_0.05_Fe sample, cyanuric acid forms. However, after 60 min, it is further degraded probably by ring opening, indicating not only that Fe-doping accelerates the conversion to cyanuric acid but also that the AB_0.05_Fe sample can further promote cyanuric acid degradation. The other two Fe-doped samples did not lead to any significant improvement in simazine degradation, indicating that a very small amount of Fe can improve the photocatalytic performance of the studied anatase/brookite TiO_2. Such a result agrees with previous literature studies on Fe-doped TiO_2, reporting that when Fe-

doping mainly occurs in the TiO_2 bulk, rather than near the surface, as with our samples, Fe sites may act as recombination centres, lowering the yield of the photocatalytic process [29].

To test the possible photo–Fenton activity of the samples under UV light, the degradation of simazine was studied in the presence of a stoichiometric amount of H_2O_2, i.e., with a simazine/H_2O_2 molar ratio of 1/20, according to Equation (22):

$$C_7H_{12}ClN_5 + 20\ H_2O_2 \rightarrow 7CO_2 + 26H_2O + 5/2N_2 + \frac{1}{2}Cl_2 \quad (22)$$

The UV-Vis spectra (not reported for the sake of brevity) showed, again, a red shift of the 222 nm band, i.e., the occurrence of the detoxication process by substitution of Cl. However, as a whole, the samples did not improve their activity in the UV/H_2O_2 system, likely due to the small amount of surface Fe. Figure 7 compares the results as a percentage of simazine degradation after 180 min in the presence of UV and UV/H_2O_2, showing that the most active sample was, again, the AB_0.05_Fe sample.

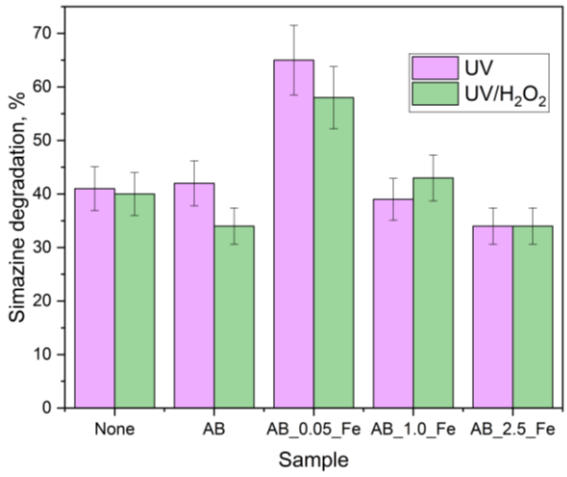

Figure 7. The percentage of simazine degradation after 180 min under UV light (purple histograms) and in the presence of UV and a stoichiometric amount of H_2O_2 (green histograms), as obtained by considering the intensity at 222 nm. An error of ±10% on the percentage of simazine degradation has been considered.

Some recent studies concern the degradation of simazine by Fenton and photo–Fenton processes in homogeneous phase: interestingly, the kinetic constant of simazine degradation by a UV/H_2O_2 system is higher than in the presence of UV/H_2O_2/Fe, likely due to a synergic effect of UV and H_2O_2, allowing a fast production of hydroxyls radicals [71]. Catalkaya et al. studied the degradation of simazine by Fenton reagent and found that the complete disappearance of simazine was achieved within 6 min reaction, but only 32% of simazine was mineralized after 15 min. This result indicates the formation of some intermediate products, which were not completely degraded to CO_2 and H_2O [34], in agreement with the extreme stability of the molecule. As a whole, our results in the heterogenous phase are promising, especially as far as the AB and the AB_0.05_Fe samples are concerned, in that we have observed that dechlorination and cyanuric formation occur, which can be useful in the perspective of detoxification processes, with the advantages of the heterogenous phase as compared to the homogeneous one [1,2].

2.3. Simazine Degradation under Simulated Solar Light

Figure S5a reports the UV-Vis spectra of the simazine solution after 5 h under 1 SUN, showing that the structure of simazine was practically unaffected by solar light and almost nihil degradation occurred. Figure S5b shows the results obtained with the mesoporous anatase used as a benchmark, with which ca. 12% simazine degradation was reached.

Figure 8 reports the spectra obtained after 5 h under 1 SUN in the presence of the 4 studied powders: with the AB sample (Figure 8a), simulated solar light brings about the decrease in the 222 nm band, from which an overall degradation of ca. 20% simazine can be reasonably estimated in this case (since no other bands formed). This result indicates that the sample can effectively exploit solar light, likely due to its absorption spectrum, (Figure 4a). This is in agreement with previous work on the degradation of N-phenylurea [11], where the occurrence of anatase/brookite heterojunctions was considered responsible of the fair activity of the anatase/brookite undoped TiO_2 under simulated solar light.

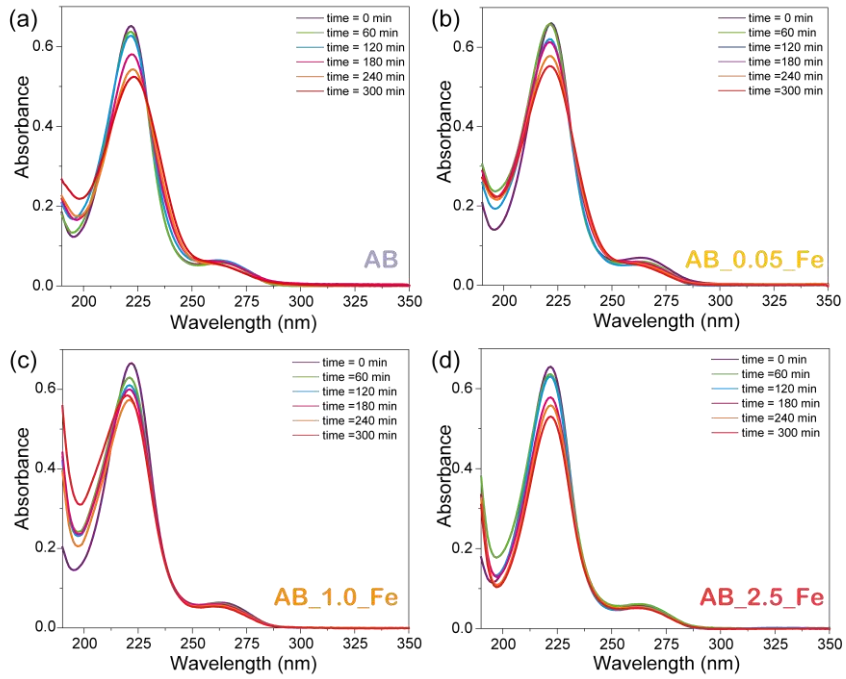

Figure 8. UV-Vis spectra of the supernatant solutions obtained after 60, 120, 180, 240 and 300 min under 1 SUN in the presence of 1 g L^{-1} AB (**a**), AB_0.05_Fe (**b**), AB_1.0_Fe (**c**) and AB_2.5_Fe (**d**) photocatalyst (t = 0 min refers to the spectrum of the fresh 1.73 × 10^{-5} M simazine solution)

It should be remarked that other materials, such as composites with relevant electrocatalytic [72] and photocatalytic applications [73,74], also present such property, i.e., the capability of accelerating interfacial charge separation, thus enhancing their electro- or photocatalytic efficiency. In the present work, this is simply obtained by a favourable alignment of the anatase and the brookite bands, as already shown in the literature with anatase and rutile polymorphs [12,75].

Unfortunately, doping with Fe does not boost the photocatalytic degradation, in that doped samples were able to degrade ca. 15–20% simazine (Figure 8b–d). To test a possible effect of surface Fe-doping in the presence of H_2O_2, ancillary experiments (not reported for the sake of brevity) were carried out under simulated solar light in the presence of a stoichiometric amount of H_2O_2, but no significant improvement was observed as compared to the tests in the absence of H_2O_2. It has to be remarked, however, that due to the high stability of the simazine molecule, most literature studies deal with its degradation under UV light in the presence of strong oxidants, such as ozone [66], and only a few papers deal with its degradation under solar light, thus the obtained results obtained under solar illumination are promising.

Interestingly, some recent literature studies concern the degradation of atrazine (a molecule similar to simazine, Scheme 2) by non-metal-doped TiO_2. With B-doped anatase/rutile mixed phases, where anatase/rutile heterojunctions occur [75], the non-metal helps stabilize the photogenerated charges; with ZnO/N-doped TiO_2 composites,

where heterojunctions can stabilize the photogenerated charges [76], the non-metal helps extend the semiconductor absorption towards the visible range. On the ground of such recent works, our results are particularly interesting in terms of the detoxification of simazine by a TiO_2 mixed phase with anatase/brookite heterojunctions and a low amount of Fe doping having a positive effect on simazine degradation. This is especially true considering the importance of detoxification, i.e., the production of less toxic molecules, in agreement with the findings in Ref. [77] where a careful toxicity evaluation was also carried out.

3. Materials and Methods

3.1. Materials Synthesis

For the synthesis of both undoped and Fe-doped TiO_2, ACS-grade chemicals purchased by Merck-Sigma-Aldrich, Schnelldorf Distribution, Schnelldorf, Germany) were used.

The undoped anatase/brookite TiO_2 mixed phase (sample AB) has been synthesized according to a template-free sol-gel method under pH control [44]. In a 150 mL beaker, 10.0 mL $Ti(OPr)_4$ (titanium(IV) isopropoxide, 97%) was mixed with 10.0 mL isopropyl alcohol (≥99.8%): the solution was then stirred for 20 min at 500 rpm, by adding 100 mL bi-distilled water during stirring. The $Ti(OPr)_4$/isopropyl alcohol/water mixture was poured into a Teflon autoclave, heated inside a stove for 5 h at 80 °C, and cooled down to room temperature. The solution pH was then changed by dropwise adding 1.0 M HNO_3 solution until a pH equal to 2.0 was obtained. At variance with Mutuma et al. [51], the acidic solution was stirred at room temperature for 20 h (instead of 24 h) to obtain a gel, which was repeatedly washed with bi-distilled water and isopropanol and centrifuged 3 times for 12 min at 12,000 rpm. Then, it was dried at 100 °C for 12 h in a stove and calcined at 200 °C for 2 h (temperature ramp = 5 °C min^{-1}) before cooling down to r.t. (temperature ramp = 5 °C min^{-1}), obtaining the AB sample. Finally, the powder was washed four times by using an ethanol/water (1/3) mixture, centrifuged for 10 min at 8000 rpm, and dried for 24 h at 60°C.

Fe-doping (samples AB_0.05, AB_1.0_Fe, and AB_2.5_Fe)was obtained by direct synthesis, with modifying the aforementioned procedure by adding proper amounts of $FeCl_3 \times 6H_2O$ (Iron(III) chloride hexahydrate, 97%) to the bi-distilled water before adding the solution to the $Ti(OPr)_4$/isopropyl alcohol mixture. The solution underwent the same thermal treatment as for the undoped sample, and finally, the pH was adjusted with 1.0 M HNO_3 solution, when necessary, depending on the acidity of the solution of $FeCl_3 \times 6H_2O$ in bi-distilled water.

A 100% anatase mesoporous TiO_2, fully characterized in previous works [11,55], was used as benchmark for the photocatalytic tests.

3.2. Materials Characterization

Powders X-ray diffraction (XRD) patterns were measured on an X'Pert Philips PW3040 diffractometer (Panalytical, Almelo, The Netherlands) employing Cu Kα radiation (2θ range = 10–100°; step = 0.026° 2θ; time per step = 0.8 s). The obtained XRD patterns were indexed by referring to the Powder Data File database (PDF 2000, International Centre of Diffraction Data, Newtown Square, PA, USA). The QPA (Quantitative Phase Analysis) was obtained according to the full-profile Rietveld method (X'Pert High Score Plus 3.0e software). The crystallite average size (D) was determined according to the Williamson-Hall plot (X'Pert High Score Plus 3.0e software).

N_2 adsorption/desorption isotherms were measured at −196 °C on powders pre-outgassed at 150 °C for 4 h to remove water and other atmospheric contaminants (Micromeritics ASAP 2020Plus, Micromeritics, Norcross, GA, USA). The Brunauer–Emmett–Teller (BET) method and the Barrett–Joyner–Halenda (BJH) method were adopted to determine the samples' Specific Surface Area (SSA) and Pore Size Distribution (PSD), respectively.

FE-SEM (Field Emission Scanning Electron Microscopy) micrographs were collected on a Merlin FESEM instrument (Carl-Zeiss AG, Oberkochen, Germany), equipped with an

EDX (Energy Dispersive X-ray Analysis) probe (Oxford instruments, Abingdon, UK) for semi-quantitative elemental analysis.

The Diffuse Reflectance (DR) UV-Vis spectra of the powders were collected on a Cary 5000 UV-Vis-NIR spectrophotometer (Varian instruments, Palo Alto, CA, USA), equipped with a DR sphere.

X-Ray Photoelectron Spectroscopy (XPS) analysis was performed on a PHI 5000 VersaProbe equipment (Physical Electronics, Feldkirchen, Germany) adopting monochromatic Al Kα radiation (1486.6 eV) as an X-ray source and a pass-energy of 187.75 eV. The spectral line shift of the C 1 s binding energy (BE) value at 284.8 eV was used to eliminate possible sample charging effects.

The powders' electrophoretic mobility was measured as a function of pH by dynamic light scattering (DLS, a Zetasizer Nano-ZS Malvern Instruments, Worcestershire, UK). In a typical experiment to determine the ζ-potential, the powders were suspended in ultrapure water and sonicated for 2 min (10 W/mL, 20 kHz, Sonoplus, Bandelin, Berlin, Germany) or magnetically stirred for 5 min. The pH was adjusted by adding either 0.1 M NaOH or 0.1 M HCl.

3.3. Simazine Degradation Tests

All the photocatalytic tests were carried out by adding a proper amount of photocatalyst (corresponding to 1.0 g L^{-1} concentration) to 40 mL of 1.73 10^{-5} M aqueous solution of simazine (natural pH = 5.5).

For the tests under UV light, a medium-pressure Hg lamp (light intensity of 55 mW·cm^{-2}, LC3, Hamamatsu Photonic, Hamamatsu, Japan) was used. A second set of experiments was made by adding a stoichiometric amount of H_2O_2.

For the photocatalytic tests under 1 SUN, a plasma lamp (LIFI STA-40, LUXIM, Santa Clara, CA, USA) was used to simulate solar light (AM 1.5 G, 100 mW cm^{-2}) under the following illumination conditions: 1 SUN, i.e., ~1000 W m^{-2} in the visible range and ~22 W m^{-2} in the UV range.

During the tests, the liquid/solid suspension inside the testing tube has been continuously stirred using a magnetic stirrer at ca. 300 rpm, as reported elsewhere [55]. The reaction mixture was not de-aerated although the reacting tube was sealed, with the consequence that the atmospheric O_2 was always present. At constant time intervals, aliquots of the suspension were withdrawn and immediately centrifuged twice at 12,000 rpm for 12 min (Thermo Fisher Scientific SL 16R centrifuge, Thermo Electron LED GmbH, Osterode am Harz, Germany) to obtain the supernatant solution, which was analysed on a UV-Vis-NIR spectrophotometer (Cary 5000, Varian Instruments, Mulgrave, Australia).

4. Conclusions

A simple, template-free sol-gel synthesis method based on pH control and mild calcination temperature was developed to dope an anatase/brookite TiO_2 mixed phase with Fe, an earth-abundant non-toxic metal. The physico-chemical characterization showed that the adopted synthesis procedure led to the production of high-surface-area mesoporous TiO_2 nanoparticles. Fe doping mostly occurred in the bulk of the TiO_2 matrix, in that XRD showed a noticeable change in the cell volume of the brookite phase, and XPS analysis was able to detect Fe at the TiO_2 surface only with the 2.5 wt.% Fe sample.

The photocatalytic degradation of simazine, a herbicide known for being a persistent pollutant with suspected toxicity to humans and the environment, has been studied as a probe reaction. Under UV light, different simazine by-products were observed as compared to mere photolysis: the best results in terms of simazine removal were obtained with the sample at 0.05% Fe, in agreement with the literature showing that higher Fe contents in the bulk of doped TiO_2 may lead to undesired recombination phenomena. In the presence of UV/H_2O_2, the samples photo–Fenton activity was very limited, likely due to the scarcity of surface Fe species.

Very interesting results were observed under simulated solar light, in that 4 samples were able to provide degradation of 15–20% simazine, after 5 h illumination, whereas solar light was unable to degrade simazine by mere photolysis. Moreover, the undoped anatase/brookite phase was the most active one under simulated solar light, likely due to the presence of an Urbach tail in its UV-Vis spectrum and to the presence of anatase/brookite heterojunctions, allowing effective exploitation of the photogenerated charge carriers, as already observed by some of us in previous work on the photocatalytic degradation of N-phenylurea.

Concerning the material optimization, future work will focus on the study of Fe contents in the 0.05–1.0 wt.% range, to test the possible effect on the samples' photocatalytic properties, as different Fe contents may also lead to noticeable effects on the anatase cell volume in terms, for instance, of isomorphic versus interstitial substitution. Regarding simazine degradation, future work will concern the study of the effect of varying pH, as it could affect the production of hydroxyl radicals and/or the simazine/surface interactions and include the study of the process in actual water samples, with emphasis on the search for optimal conditions to achieve detoxification.

Supplementary Materials: The following supporting information can be downloaded at: https://www.mdpi.com/article/10.3390/catal13040667/s1, Figure S1: Overlapped and single-element EDX maps of Ti, O and Fe with the following samples: (a) AB_0.05_Fe; (b) AB_1.0_Fe; (c) AB_2.5_Fe. The maps of C and Cl are not reported, as the elements occurred in traces. Figure S2: XPS survey spectra of the studied samples, showing that surface Fe species were detected only with the AB_2.5_Fe sample. Figure S3: DR UV-Vis spectra of the AB powder and of a Degussa P25 commercial powder, showing that the former has an Urbach tail, absent with the latter. Figure S4: UV-Vis spectra of the supernatant solutions obtained after 60, 120, and 180 min under UV illumination in the absence of any photocatalyst (a) and in the presence of 1 g/L mesoporous anatase (b). In both graphs, time = 0 min refers to the spectrum of the fresh 1.73×10^{-5} M simazine solution. Figure S5: UV-Vis spectra of the supernatant solutions obtained after 60, 120, 180, 240, and 300 min under 1 SUN in the absence of any photocatalyst (a) and in the presence of 1 g/L mesoporous anatase (b). In both graphs, time = 0 min refers to the spectrum of the fresh 1.73 10^{-5} M simazine solution.

Author Contributions: Conceptualization, B.B. and F.S.F.; methodology, B.B.; formal analysis, S.G. (Stefano Gervasi) and S.G. (Salvatore Guastella); investigation, S.G. (Stefano Gervasi), N.B., S.G. (Salvatore Guastella) and F.S.F.; data curation, S.G. (Stefano Gervasi), F.S.F. and N.B.; writing—original draft preparation, B.B.; writing—review and editing N.B. and F.S.F.; supervision, N.B., F.S.F. and B.B.; funding acquisition, B.B. All authors have read and agreed to the published version of the manuscript.

Funding: This research was funded by the program PNRR Mac-2 NODES Nord Ovest Digitale e Sostenibile and Agritech National Research Center and received funding from the European Union Next-Generation EU (PIANO NAZIONALE DI RIPRESA E RESILIENZA (PNRR)—MISSIONE 4 COMPONENTE 2, INVESTIMENTO 1.4—D.D. 1032 17/06/2022, CN00000022). This manuscript reflects only the authors' views and opinions, neither the European Union nor the European Commission can be considered responsible for them

Data Availability Statement: Not applicable.

Acknowledgments: The authors thank M. Sangermano (Department of Applied Science and Technology, Politecnico di Torino) for lending the UV lamp, S. Hernandez (Department of Applied Science and Technology, Politecnico di Torino) for lending the solar lamp, and T. Tosco (Department of Environment, Land and Infrastructure Engineering, Politecnico di Torino) for providing access to electrophoretic measurements.

Conflicts of Interest: The authors declare no conflict of interest.

References

1. Freyria, F.S.; Armandi, M.; Compagnoni, M.; Ramis, G.; Rossetti, I.; Bonelli, B. Catalytic and Photocatalytic Processes for the Abatement of N-Containing Pollutants from Wastewater. Part 2: Organic Pollutants. *J. Nanosci. Nanotechnol.* **2017**, *17*, 3654–3672. [CrossRef]
2. Compagnoni, M.; Ramis, G.; Freyria, F.S.; Armandi, M.; Bonelli, B.; Rossetti, I. Photocatalytic Processes for the Abatement of N-Containing Pollutants from Waste Water. Part 1: Inorganic Pollutants. *J. Nanosci. Nanotechnol.* **2017**, *17*, 3632–3653. [CrossRef]
3. Ozawa, K.; Emori, M.; Yamamoto, S.; Yukawa, R.; Yamamoto, S.; Hobara, R.; Fujikawa, K.; Sakama, H.; Matsuda, I. Electron-hole recombination time at TiO_2 single-crystal surfaces: Influence of surface band bending. *J. Phys. Chem. Lett.* **2014**, *5*, 1953–1957. [CrossRef] [PubMed]
4. Guayaquil-Sosa, J.F.; Serrano-Rosales, B.; Valadés-Pelayo, P.J.; de Lasa, H. Photocatalytic hydrogen production using mesoporous TiO_2 doped with Pt. *Appl. Catal. B Environ.* **2017**, *211*, 337–348. [CrossRef]
5. Lavorato, C.; Argurio, P.; Mastropietro, T.F.; Pirri, G.; Poerio, T.; Molinari, R. Pd/TiO_2 doped faujasite photocatalysts for acetophenone transfer hydrogenation in a photocatalytic membrane reactor. *J. Catal.* **2017**, *353*, 152–161. [CrossRef]
6. Di Paola, A.; Bellardita, M.; Palmisano, L. Brookite, the Least Known TiO_2 Photocatalyst. *Catalysts* **2013**, *3*, 36–73. [CrossRef]
7. Manzoli, M.; Freyria, F.S.; Blangetti, N.; Bonelli, B. Brookite, a sometimes under evaluated TiO_2 polymorph. *RSC Adv.* **2022**, *12*, 3322–3334. [CrossRef]
8. Liu, Y.; Wang, Z.; Huang, W. Influences of TiO_2 phase structures on the structures and photocatalytic hydrogen production of CuO_x/TiO_2 photocatalysts. *Appl. Surf. Sci.* **2016**, *389*, 760–767. [CrossRef]
9. Liu, Y.; Ye, Z.; Li, D.; Wang, M.; Zhang, Y.; Huang, W. Tuning CuO_x-TiO_2 interaction and photocatalytic hydrogen production of CuO_x/TiO_2 photocatalysts via TiO_2 morphology engineering. *Appl. Surf. Sci.* **2019**, *473*, 500–510. [CrossRef]
10. Bonelli, B.; Esposito, S.; Freyria, F.S. Mesoporous Titania: Synthesis, properties and comparison with non-porous titania. In *Titanium Dioxide*; Janus, M., Ed.; Intech: London, UK, 2017; ISBN 978-953-51-5493-8.
11. Freyria, F.S.; Blangetti, N.; Esposito, S.; Nasi, R.; Armandi, M.; Annelio, V.; Bonelli, B. Effects of the Brookite Phase on the Properties of Different Nanostructured TiO_2 Phases Photocatalytically Active Towards the Degradation of N-Phenylurea. *ChemistryOpen* **2020**, *9*, 903–912. [CrossRef]
12. Fang, J.; Wang, F.; Qian, K.; Bao, H.; Jiang, Z.; Huang, W. Bifunctional N-Doped Mesoporous TiO_2 Photocatalysts. *J. Phys. Chem. C* **2008**, *112*, 18150–18156. [CrossRef]
13. Hossain, M.A.; Elias, M.; Sarker, D.R.; Diba, Z.R.; Mithun, J.M.; Azad, M.A.K.; Siddiquey, I.A.; Rahman, M.M.; Uddin, J.; Uddin, M.N. Synthesis of Fe- or Ag-doped TiO_2–MWCNT nanocomposite thin films and their visible-light-induced catalysis of dye degradation and antibacterial activity. *Res. Chem. Intermed.* **2018**, *44*, 2667–2683. [CrossRef]
14. Ohno, T.; Tokieda, K.; Higashida, S.; Matsumura, M. Synergism between rutile and anatase TiO_2 particles in photocatalytic oxidation of naphthalene. *Appl. Catal. A Gen.* **2003**, *244*, 383–391. [CrossRef]
15. Jiang, X.; Manawan, M.; Feng, T.; Qian, R.; Zhao, T.; Zhou, G.; Kong, F.; Wang, Q.; Dai, S.; Pan, J.H. Anatase and rutile in evonik aeroxide P25: Heterojunctioned or individual nanoparticles? *Catal. Today* **2018**, *300*, 12–17. [CrossRef]
16. Manga Raju, I.; Siva Rao, T.; Divya Lakshmi, K.V.; Ravi Chandra, M.; Swathi Padmaja, J.; Divya, G. Poly 3-Thenoic acid sensitized, Copper doped anatase/brookite TiO_2 nanohybrids for enhanced photocatalytic degradation of an organophosphorus pesticide. *J. Environ. Chem. Eng.* **2019**, *7*, 103211. [CrossRef]
17. Tay, Q.; Wang, X.; Zhao, X.; Hong, J.; Zhang, Q.; Xu, R.; Chen, Z. Enhanced visible light hydrogen production via a multiple heterojunction structure with defect-engineered g-C_3N_4 and two-phase anatase/brookite TiO_2. *J. Catal.* **2016**, *342*, 55–62. [CrossRef]
18. Zhao, B.; Chen, F.; Jiao, Y.; Yang, H.; Zhang, J. Ag^0-loaded brookite/anatase composite with enhanced photocatalytic performance towards the degradation of methyl orange. *J. Mol. Catal. A Chem.* **2011**, *348*, 114–119. [CrossRef]
19. Panov, G.I.; Sheveleva, G.A.; Kharitonov, A.S.; Romannikov, V.N.; Vostrikova, L.A. Oxidation of benzene to phenol by nitrous oxide over Fe-ZSM-5 zeolites. *Appl. Catal. A Gen.* **1992**, *82*, 31–36. [CrossRef]
20. Bahadori, E.; Vaiano, V.; Esposito, S.; Armandi, M.; Sannino, D.; Bonelli, B. Photo-activated degradation of tartrazine by H_2O_2 as catalyzed by both bare and Fe-doped methyl-imogolite nanotubes. *Catal. Today* **2018**, *304*, 199–207. [CrossRef]
21. Shafia, E.; Esposito, S.; Armandi, M.; Bahadori, E.; Garrone, E.; Bonelli, B. Reactivity of bare and Fe-doped alumino-silicate nanotubes (imogolite) with H_2O_2 and the azo-dye Acid Orange 7. *Catal. Today* **2016**, *277*, 89–96. [CrossRef]
22. Mardani, H.R.; Forouzani, M.; Ziari, M.; Biparva, P. Visible light photo-degradation of methylene blue over Fe or Cu promoted ZnO nanoparticles. *Spectrochim. Acta—Part A Mol. Biomol. Spectrosc.* **2015**, *141*, 27–33. [CrossRef] [PubMed]
23. Zhang, W.; Zhao, J.; Liu, Z.; Liu, Z. Structural, optical and magnetic properties of Zn_{1-x} Fe_x O powders by sol-gel method. *Appl. Surf. Sci.* **2013**, *284*, 49–52. [CrossRef]
24. Ciciliati, M.A.; Silva, M.F.; Fernandes, D.M.; De Melo, M.A.C.; Hechenleitner, A.A.W.; Pineda, E.A.G. Fe-doped ZnO nanoparticles: Synthesis by a modified sol-gel method and characterization. *Mater. Lett.* **2015**, *159*, 84–86. [CrossRef]
25. Yu, J.; Xiang, Q.; Zhou, M. Preparation, characterization and visible-light-driven photocatalytic activity of Fe-doped titania nanorods and first-principles study for electronic structures. *Appl. Catal. B Environ.* **2009**, *90*, 595–602. [CrossRef]
26. Tong, T.; Zhang, J.; Tian, B.; Chen, F.; He, D. Preparation of Fe^{3+}-doped TiO_2 catalysts by controlled hydrolysis of titanium alkoxide and study on their photocatalytic activity for methyl orange degradation. *J. Hazard. Mater.* **2008**, *155*, 572–579. [CrossRef] [PubMed]

27. Khan, H.; Khan Swati, I. Fe^{3+}-doped Anatase TiO_2 with d−d Transition, Oxygen Vacancies and Ti^{3+} Centers: Synthesis, Characterization, UV−vis Photocatalytic and Mechanistic Studies. *Ind. Eng. Chem. Res.* **2016**, *55*, 6619–6633. [CrossRef]
28. Sood, S.; Umar, A.; Mehta, S.K.; Kansal, S.K. Highly effective Fe-doped TiO_2 nanoparticles photocatalysts for visible-light driven photocatalytic degradation of toxic organic compounds. *J. Colloid Interface Sci.* **2015**, *450*, 213–223. [CrossRef]
29. Komaraiah, D.; Radha, E.; Sivakumar, J.; Sayanna, R. Influence of Fe^{3+}ions on the optical properties and photocatalytic ability of spin coated Fe^{3+}doped brookite TiO_2 thin films. *Funct. Compos. Struct.* **2022**, *4*, 15010. [CrossRef]
30. Ramirez, J.H.; Maldonado-Hódar, F.J.; Pérez-Cadenas, A.F.; Moreno-Castilla, C.; Costa, C.A.; Madeira, L.M. Azo-dye Orange II degradation by heterogeneous Fenton-like reaction using carbon-Fe catalysts. *Appl. Catal. B Environ.* **2007**, *75*, 312–323. [CrossRef]
31. Neyens, E.; Baeyens, J. A review of classic Fenton's peroxidation as an advanced oxidation technique. *J. Hazard. Mater.* **2003**, *98*, 33–50. [CrossRef]
32. Pignatello, J.J.; Oliveros, E.; MacKay, A. Advanced oxidation processes for organic contaminant destruction based on the fenton reaction and related chemistry. *Crit. Rev. Environ. Sci. Technol.* **2006**, *36*, 1–84. [CrossRef]
33. Rahim Pouran, S.; Abdul Aziz, A.R.; Wan Daud, W.M.A. Review on the main advances in photo-Fenton oxidation system for recalcitrant wastewaters. *J. Ind. Eng. Chem.* **2015**, *21*, 53–69. [CrossRef]
34. Catalkaya, E.C.; Kargi, F. Advanced oxidation and mineralization of simazine using Fenton's reagent. *J. Hazard. Mater.* **2009**, *168*, 688–694. [CrossRef] [PubMed]
35. Klavarioti, M.; Mantzavinos, D.; Kassinos, D. Removal of residual pharmaceuticals from aqueous systems by advanced oxidation processes. *Environ. Int.* **2009**, *35*, 402–417. [CrossRef] [PubMed]
36. Catalkaya, E.C.; Kargi, F. Degradation and Mineralization of Simazine in Aqueous Solution by Ozone/Hydrogen Peroxide Advanced Oxidation. *J. Environ. Eng.* **2009**, *135*, 1357–1364. [CrossRef]
37. European Union. Council Directive 91/414/EEC of 15 July 1991 concerning the placing of plant protection products on the market. *Off. J. Eur. Union* **2010**, 1–32.
38. Grasselli, F.; Bussolati, S.; Ramoni, R.; Grolli, S.; Basini, G. Simazine, a triazine herbicide, disrupts swine granulosa cell functions. *Anim. Reprod.* **2018**, *15*, 3–11. [CrossRef]
39. Endocrine-Disrupting Pesticide Atrazine to Be Banned in Hawaii, Five U.S. Territories, Prohibited on Conifers, Roadsides. Available online: https://biologicaldiversity.org/w/news/press-releases/endocrine-disrupting-pesticide-atrazine-be-banned-hawaii-five-us-territories-prohibited-conifers-roadsides-2020-09-23/ (accessed on 23 September 2020).
40. Rao, Y.; Chu, W. Visible light-induced photodegradation of simazine in aqueous TiO_2 suspension. *Ind. Eng. Chem. Res.* **2013**, *52*, 13580–13586. [CrossRef]
41. Mohaupt, V.; Völker, J.; Altenburger, R.; Birk, S.; Kirst, I.; Kühnel, D.; Küster, E.; Semerádová, S.; Šubelj, G.; Whalley, C. *Pesticides in European Rivers, Lakes and Groundwaters—Data Assessment*; ETC/ICM: Magdeburg, Germany, 2020.
42. Stefano, P.H.P.; Roisenberg, A.; Santos, M.R.; Dias, M.A.; Montagner, C.C. Unraveling the occurrence of contaminants of emerging concern in groundwater from urban setting: A combined multidisciplinary approach and self-organizing maps. *Chemosphere* **2022**, *299*, 134395. [CrossRef]
43. Esquerdo, A.A.; Rico, D.P.; Galvañ, P.J.V.; Gadea, I.S. Activated carbon and ozone to reduce simazine in water. *Water* **2020**, *12*, 2900. [CrossRef]
44. Loiseau, T.; Serre, C.; Huguenard, C.; Fink, G.; Taulelle, F.; Henry, M.; Bataille, T.; Férey, G. A Rationale for the Large Breathing of the Porous Aluminum Terephthalate (MIL-53) Upon Hydration. *Chem.—A Eur. J.* **2004**, *10*, 1373–1382. [CrossRef] [PubMed]
45. Sun, Z.; Zheng, S.; Ayoko, G.A.; Frost, R.L.; Xi, Y. Degradation of simazine from aqueous solutions by diatomite-supported nanosized zero-valent iron composite materials. *J. Hazard. Mater.* **2013**, *263*, 768–777. [CrossRef] [PubMed]
46. Flores, K.; Valdes, C.; Ramirez, D.; Eubanks, T.M.; Lopez, J.; Hernandez, C.; Alcoutlabi, M.; Parsons, J.G. The effect of hybrid zinc oxide/graphene oxide (ZnO/GO) nano-catalysts on the photocatalytic degradation of simazine. *Chemosphere* **2020**, *259*, 127414. [CrossRef] [PubMed]
47. Boruah, P.K.; Darabdhara, G.; Das, M.R. Polydopamine functionalized graphene sheets decorated with magnetic metal oxide nanoparticles as efficient nanozyme for the detection and degradation of harmful triazine pesticides. *Chemosphere* **2021**, *268*, 129328. [CrossRef]
48. Suhaimy, S.H.M.; Lai, C.W.; Tajuddin, H.A.; Samsudin, E.M.; Johan, M.R. Impact of TiO_2 nanotubes' morphology on the photocatalytic degradation of simazine pollutant. *Materials* **2018**, *11*, 2066. [CrossRef]
49. Meriam Suhaimy, S.; Abd Hamid, S.; Lai, C.; Hasan, M.; Johan, M. TiO_2 Nanotubes Supported Cu Nanoparticles for Improving Photocatalytic Degradation of Simazine under UV Illumination. *Catalysts* **2016**, *6*, 167. [CrossRef]
50. Evgenidou, E.; Fytianos, K. Photodegradation of Triazine Herbicides in Aqueous Solutions and Natural Waters. *J. Agric. Food Chem.* **2002**, *50*, 6423–6427. [CrossRef]
51. Mutuma, B.K.; Shao, G.N.; Kim, W.D.; Kim, H.T. Sol–gel synthesis of mesoporous anatase–brookite and anatase–brookite–rutile TiO_2 nanoparticles and their photocatalytic properties. *J. Colloid Interface Sci.* **2015**, *442*, 1–7. [CrossRef]
52. Mancuso, A.; Sacco, O.; Vaiano, V.; Bonelli, B.; Esposito, S.; Freyria, F.S.; Blangetti, N.; Sannino, D. Visible Light-Driven Photocatalytic Activity and Kinetics of Fe-Doped TiO_2 Prepared by a Three-Block Copolymer Templating Approach. *Materials* **2021**, *14*, 3105. [CrossRef]

53. Mancuso, A.; Blangetti, N.; Sacco, O.; Freyria, F.S.; Bonelli, B.; Esposito, S.; Sannino, D.; Vaiano, V. Photocatalytic Degradation of Crystal Violet Dye under Visible Light by Fe-Doped TiO_2 Prepared by Reverse-Micelle Sol–Gel Method. *Nanomaterials* **2023**, *13*, 270. [CrossRef]
54. Piumetti, M.; Freyria, F.S.; Armandi, M.; Geobaldo, F.; Garrone, E.; Bonelli, B. Fe- and V-doped mesoporous titania prepared by direct synthesis: Characterization and role in the oxidation of AO7 by H_2O_2 in the dark. *Catal. Today* **2014**, *227*, 71–79. [CrossRef]
55. Freyria, F.; Compagnoni, M.; Ditaranto, N.; Rossetti, I.; Piumetti, M.; Ramis, G.; Bonelli, B. Pure and Fe-Doped Mesoporous Titania Catalyse the Oxidation of Acid Orange 7 by H_2O_2 under Different Illumination Conditions: Fe Doping Improves Photocatalytic Activity under Simulated Solar Light. *Catalysts* **2017**, *7*, 213. [CrossRef]
56. Soo, C.W.; Juan, J.C.; Lai, C.W.; Hamid, S.B.A.; Yusop, R.M. Fe-doped mesoporous anatase-brookite titania in the solar-light-induced photodegradation of Reactive Black 5 dye. *J. Taiwan Inst. Chem. Eng.* **2016**, *68*, 153–161. [CrossRef]
57. Sannino, F.; Pansini, M.; Marocco, A.; Bonelli, B.; Garrone, E.; Esposito, S. The role of outer surface/inner bulk Brønsted acidic sites in the adsorption of a large basic molecule (simazine) on H-Y zeolite. *Phys. Chem. Chem. Phys.* **2015**, *17*, 28950–28957. [CrossRef]
58. López, R.; Gómez, R. Photocatalytic Degradation of 4-Nitrophenol on Well Characterized Sol-Gel Molybdenum Doped Titania Semiconductors. *Top. Catal.* **2011**, *54*, 504–511. [CrossRef]
59. Yaghoubi, H.; Li, Z.; Chen, Y.; Ngo, H.T.; Bhethanabotla, V.R.; Joseph, B.; Ma, S.; Schlaf, R.; Takshi, A. Toward a Visible Light-Driven Photocatalyst: The Effect of Midgap-States-Induced Energy Gap of Undoped TiO_2 Nanoparticles. *ACS Catal.* **2015**, *5*, 327–335. [CrossRef]
60. Blangetti, N.; Freyria, F.S.; Calviello, M.C.; Ditaranto, N.; Guastella, S.; Bonelli, B. Photocatalytic Degradation of Paracetamol under Simulated Sunlight by Four TiO_2 Commercial Powders: An Insight into the Performance of Two Sub-Micrometric Anatase and Rutile Powders and a Nanometric Brookite Powder. *Catalysts* **2023**, *13*, 434. [CrossRef]
61. Mustafa, S.; Tasleem, S.; Naeem, A. Surface charge properties of Fe_2O_3 in aqueous and alcoholic mixed solvents. *J. Colloid Interface Sci.* **2004**, *275*, 523–529. [CrossRef] [PubMed]
62. Holmberg, J.P.; Ahlberg, E.; Bergenholtz, J.; Hassellöv, M.; Abbas, Z. Surface charge and interfacial potential of titanium dioxide nanoparticles: Experimental and theoretical investigations. *J. Colloid Interface Sci.* **2013**, *407*, 168–176. [CrossRef]
63. Nasi, R.; Sannino, F.; Picot, P.; Thill, A.; Oliviero, O.; Esposito, S.; Armandi, M.; Bonelli, B. Hybrid organic-inorganic nanotubes effectively adsorb some organic pollutants in aqueous phase. *Appl. Clay Sci.* **2020**, *186*, 105449. [CrossRef]
64. Liu, Y.; Zhu, K.; Su, M.; Zhu, H.; Lu, J.; Wang, Y.; Dong, J.; Qin, H.; Wang, Y.; Zhang, Y. Influence of solution pH on degradation of atrazine during UV and UV/H_2O_2 oxidation: Kinetics, mechanism, and degradation pathways. *RSC Adv.* **2019**, *9*, 35847–35861. [CrossRef] [PubMed]
65. Hu, J.-Y.; Morita, T.; Magara, Y.; Aizawa, T. Evaluation of the Reactivity of Pesticides with Ozone in Water using the Energies of Frontier Molecular Orbitals. *Water Res.* **2000**, *34*, 2215–2222. [CrossRef]
66. Rivas, F.J.; Navarrete, V.; Beltrán, F.J.; García-Araya, J.F. Simazine Fenton's oxidation in a continuous reactor. *Appl. Catal. B Environ.* **2004**, *48*, 249–258. [CrossRef]
67. Cantú, R.; Evans, O.; Kawahara, F.K.; Shoemaker, J.A.; Dufour, A.P. An HPLC Method with UV Detection, pH Control, and Reductive Ascorbic Acid for Cyanuric Acid Analysis in Water. *Anal. Chem.* **2000**, *72*, 5820–5828. [CrossRef]
68. Mu, Y.; Chen, Y.; Fu, Q.; He, P.Y.; Sun, Q.; Zou, J.P.; Zhang, L.; Wang, D.; Luo, S. Transformation of Atrazine to Hydroxyatrazine with Alkali-H_2O_2 Treatment: An Efficient Dechlorination Strategy under Alkaline Conditions. *ACS Water* **2021**, *1*, 1868–1877. [CrossRef]
69. Mu, Y.; Zhan, G.; Huang, C.; Wang, X.; Ai, Z.; Zou, J.; Luo, S.; Zhang, L. Dechlorination-Hydroxylation of Atrazine to Hydroxyatrazine with Thiosulfate: A Detoxification Strategy in Seconds. *Environ. Sci. Technol.* **2019**, *53*, 3208–3216. [CrossRef] [PubMed]
70. Moreira, A.J.; Borges, A.C.; Gouvea, L.F.C.; MacLeod, T.C.O.; Freschi, G.P.G. The process of atrazine degradation, its mechanism, and the formation of metabolites using UV and UV/MW photolysis. *J. Photochem. Photobiol. A Chem.* **2017**, *347*, 160–167. [CrossRef]
71. Lojo-López, M.; Andrades, J.A.; Egea-Corbacho, A.; Coello, M.D.; Quiroga, J.M. Degradation of simazine by photolysis of hydrogen peroxide Fenton and photo-Fenton under darkness, sunlight and UV light. *J. Water Process Eng.* **2021**, *42*, 102115. [CrossRef]
72. Cao, Q.; Hao, S.; Wu, Y.; Pei, K.; You, W.; Che, R. Interfacial charge redistribution in interconnected network of Ni_2P–Co_2P boosting electrocatalytic hydrogen evolution in both acidic and alkaline conditions. *Chem. Eng. J.* **2021**, *424*, 130444. [CrossRef]
73. Cao, Q.; Li, Q.; Pi, Z.; Zhang, J.; Sun, L.-W.; Xu, J.; Cao, Y.; Cheng, J.; Bian, Y. Metal–Organic-Framework-Derived Ball-Flower-like Porous Co_3O_4/Fe_2O_3 Heterostructure with Enhanced Visible-Light-Driven Photocatalytic Activity. *Nanomaterials* **2022**, *12*, 904. [CrossRef]
74. Zhang, Z.; Zhang, Y.; Han, X.; Guo, L.; Wang, D.; Lv, K. Assembly of $CaIn_2S_4$ on Defect-Rich BiOCl for Acceleration of Interfacial Charge Separation and Photocatalytic Phenol Degradation via S-Scheme Electron Transfer Mechanism. *Catalysts* **2021**, *11*, 1130. [CrossRef]
75. Hurum, D.C.; Agrios, A.G.; Gray, K.A.; Rajh, T.; Thurnauer, M.C. Explaining the Enhanced Photocatalytic Activity of Degussa P25 Mixed-Phase TiO_2 Using EPR. *J. Phys. Chem. B* **2003**, *107*, 4545–4549. [CrossRef]

76. Navarra, W.; Ritacco, I.; Sacco, O.; Caporaso, L.; Farnesi Camellone, M.; Venditto, V.; Vaiano, V. Density Functional Theory Study and Photocatalytic Activity of ZnO/N-Doped TiO_2 Heterojunctions. *J. Phys. Chem. C* **2022**, *126*, 7000–7011. [CrossRef]
77. Navarra, W.; Sacco, O.; Daniel, C.; Venditto, V.; Vaiano, V.; Vignette, D.A.L.; Bojic, C.; Libralato, G.; Lofrano, G.; Carotenuto, M. Photocatalytic degradation of atrazine by an N-doped TiO_2/polymer composite: Catalytic efficiency and toxicity evaluation. *J. Environ. Chem. Eng.* **2022**, *10*, 108167. [CrossRef]